Geophysical Prospecting 39, 827–844, 1991

DAMPED LEAST-SQUARES INVERSION OF TIME-DOMAIN AIRBORNE EM DATA BASED ON SINGULAR VALUE DECOMPOSITION[1]

H. HUANG[2] and G. J. PALACKY[3]

ABSTRACT

HUANG, H. and PALACKY, G.J. 1991. Damped least-squares inversion of time-domain airborne EM data based on singular value decomposition. *Geophysical Prospecting* 39, 827–844.

Airborne electromagnetic (AEM) methods are increasingly being used as tools of geological mapping, groundwater exploration and prospecting for coal and lignite. In such applications, quantitative interpretation is commonly based on the layered-earth model. A new approach, a damped least-squares inversion with singular value decomposition, is proposed for interpretation of time-domain, towed-bird AEM data. Studies using theoretical and field AEM data indicate that inversion techniques are dependable and provide fast converging solutions. An analysis has been made of the accuracy of model parameter determination, which depends on resistivity and thickness distribution. In the common case of conductive overburden, upper-layer resistivity and thickness are usually well determined, although situations exist where their separation becomes difficult. In the case of a resistive layer overlying a conductive basement, the layer thickness is the best-determined parameter. In both cases, estimates of basement resistivity are the least reliable. Field data obtained with the Chinese-made M-1 AEM system in Dongling, Anhui Province, China, were processed using the described inversion algorithm. The survey area comprised fluvial Cenozoic clays and weathered Mesozoic sediments. Inversion of AEM data resulted in accurate depth-to-bedrock sections and realistic estimates of the resistivities of overburden and bedrock which agree with the results of drilling and resistivity sounding.

INTRODUCTION

The first airborne electromagnetic (AEM) systems, which were developed in the early 1950s, were used primarily in prospecting for massive sulphide deposits. Such targets stand out when embedded in a resistive medium and can be easily recognized in the absence of conductive overburden. With improvements in instrumentation, other applications requiring more sophisticated interpretation have become possible, notably groundwater exploration (Baudoin, Durozoy and Utard 1970),

[1] Received January 1990, revision accepted February 1991.

[2] Changchun University of Earth Sciences, Department of Applied Geophysics, 6 Ximinzhu Street, Changchun, Jilin 130026, China.

[3] Geological Survey of Canada, 601 Booth Street, Ottawa, Ontario, Canada K1A 0E8.

kimberlite prospecting (Macnae 1979), geological mapping (Palacky 1981, 1987), coal and lignite prospecting (Huang and Wang 1985a), identification of areas affected by salinization (O'Connell and Nader 1986), shallow-ocean bathymetry (Zollinger *et al.* 1987) and sea-ice thickness determinations (Kovacs, Valleau and Holladay 1987). In these applications there is a need for continuous determination of certain parameters (e.g. depth, resistivity) rather than for quantitative interpretation of selected anomalies which is the norm in mineral exploration. Among researchers pioneering resistivity mapping was Fraser (1978) who developed a computer routine for obtaining overburden resistivity and bedrock depth information from multicoil helicopter AEM data. Inversion of helicopter AEM data using horizontal layer models has been described by Paterson and Reford (1986).

Interpretation of time-domain AEM data assuming a layered model has been treated by Becker (1969), Nelson and Morris (1969), Palacky and West (1973) and Dyck, Becker and Collett (1974). The last two also included examples of field data interpretation. De Moully and Becker (1984) argued that a computerized matching of field data with selected nomograms is more efficient than a true inversion. Their approach has been favoured by North American contractors. O'Connell and Nader (1986) published several examples of computer interpretation of field time-domain AEM data.

The potential for using inversion techniques in the interpretation of time-domain AEM data has been studied during the last 10 years in China and Canada. The material presented here is the result of research at the Changchun University of Earth Sciences. Studies on the transformation of AEM responses to resistivity sections have been carried out in China since the early 1980s and the results have been reported in Chinese journals (Huang *et al.* 1983; Huang and Wang 1985b). Until recently, scientists in China had only limited opportunities to discuss research with their colleagues in the West, and therefore their results did not have the impact they probably deserved.

Both Chinese and Canadian research groups tried to focus on problems arising from their specific application needs. While the search for massive sulphide deposits remained a priority application of AEM methods in Canada, Chinese geophysicists began to appreciate the potential of AEM techniques for geological mapping and environmental investigations (Huang 1986). In Canada, McGill University in Montreal was the first institution to carry out research in the field of time-domain AEM data inversion. Keating and Crossley (1990) developed inversion routines for the plate model. The response of conductive massive sulphide deposits, which are often tabular in shape and small in size, can be conveniently approximated by vertical or dipping plates. Barongo (1989) investigated the possibility of using inversion of time-domain AEM data to generate apparent resistivity maps. Such products can be used in mapping bedrock lithology in tropical environments.

This paper proposes an interpretation method based on damped least-squares inversion and singular value decomposition (SVD). The principles of the technique, which is at present widely used in other geophysical disciplines, were described by Jackson (1972) and Wiggins (1972). Recently, inversion problems were treated by Menke (1984).

The M-1 AEM System

The first time-domain AEM system, INPUT (INduced PUlse Transient), registered trademark of Barringer Research Ltd was developed by Dr A. R. Barringer in 1959 (Collett 1986). The transmitter was formed by a large loop, mounted in a fixed-wing aircraft, and the receiver was suspended in a 'bird' towed by the plane. The primary electromagnetic field was generated in short pulses (approximately 1 ms long) followed by transmitter-off periods. The e.m.f. due to the secondary magnetic field was measured during those periods at six time intervals of varying length (channels). Systems sharing the same design but differing in technical details (such as the number of channels or the duration of the primary pulse) were built in the U.S.S.R. (AMPP-2), India (NGRI), China (M-1) and Canada (GEOTEM, QUESTEM). In the 1970s and early 1980s, time-domain AEM systems accounted for about two-thirds of all AEM surveys world-wide (Palacky 1986).

A field example obtained with the M-1 system developed at the Changchun University of Earth Sciences is given. The first prototype of the system became operational in 1977 (Zheng and Wang 1979). The transmitter is a seven-turn, vertical-axis loop mounted on a fixed-wing aircraft. A maximum dipole moment of 70 000 Am^2 is generated by injecting a peak current of approximately 160 A. The receiver is a horizontal-axis coil towed in a 'bird', nominally 90 m behind and 63 m below the aircraft (Fig. 1). The system was designed for optimum performance at a terrain clearance of 120 m, but in practice the flight altitude during surveys in China was often much higher. The primary pulse of 1 ms duration has a half-sine form and is followed by a 2.6 ms off-period. The mean positions of the window centres (channels) at which the signal is measured at the receiver are 0.3, 0.5, 0.8, 1.2, 1.7 and 2.3 ms after the transmitter switch-off (delay time). The width of the non-overlapping windows increases in steps from 0.2 to 0.6 ms. The noise level of the system decreases with the delay time from approximately 100 parts per million

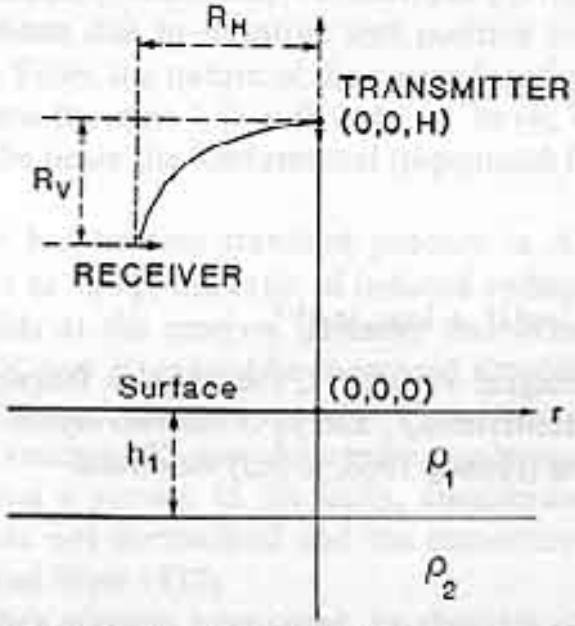

FIG. 1. Sketch of the time-domain, towed-bird AEM system used in the theoretical studies. The interpretation model is a two-layer earth; the coordinate system is cylindrical.

(ppm) of the ratio, secondary to primary field, on channel 1 to 5 ppm on channel 6 (peak to peak). However, because the AEM response at high channels is much weaker for most conductors (except those possessing high conductivity), the signal-to-noise ratio may actually deteriorate with increasing delay time.

The Forward Problem

Several researchers have solved the EM response of a layered earth for dipole source excitation (Wait 1958; Ward 1971; Frischknecht 1967; Becker 1969; Nelson and Morris 1969). The most recent treatment was given by Ward and Hohmann (1988). In order to avoid details which would have little relevance to the main thrust of this paper, only the basic equations essential to the understanding of the time-domain AEM problem will be presented here.

The transmitter–receiver geometry and a two-layer earth model are shown in Fig. 1. The transmitter is at a height H above the origin of the cylindrical co-ordinate system (r, ϕ, z). According to Huang (1986, p. 59), the secondary radial magnetic field H_{zr} for a layered earth is

$$H_{zr} = \frac{M_z}{4\pi} \int_0^{\infty} M(\lambda) \exp\left[\lambda(z + H)\right] \lambda^2 J_1(\lambda r)\, d\lambda \qquad (1)$$

$$= \frac{M_z}{4\pi} D,$$

where M_z is the magnetic moment of the transmitter and J_1 is the Bessel function of the first kind of order one. The term $M(\lambda)$ can be written as

$$M(\lambda) = \frac{(1 - \lambda C_1)}{(1 + \lambda C_1)}, \qquad (2)$$

where, for a two-layer earth, C_1 is given by

$$C_1 = \frac{C_2 + \tanh(\alpha_1 h_1)/\alpha_1}{1 + \alpha_1 C_2 \tanh(\alpha_1 h_1)} \qquad (3)$$

and

$$C_2 = (\lambda^2 + i\omega\mu_0/\rho_2)^{-1/2}, \qquad \alpha_1 = (\lambda^2 + i\omega\mu_0/\rho_1)^{1/2}.$$

C_1 is a complex function of an integral variable λ, the angular frequency ω, the magnetic permeability μ_0 and the resistivities ρ_1 and ρ_2 of the two layers.

Writing (1) as a complex function (Huang 1986, p. 161) we obtain

$$H_{zr} = \frac{M_z}{4\pi} |D| \exp(i\phi).$$

Taking the Fourier transform of the equation, a solution is obtained in the time domain, i.e.

$$H_z(t) = \frac{M_z}{2\pi} \sum_{k=1,3,\ldots}^{\infty} S_k |D_k| \cos(k\omega_0 t + \phi_k), \qquad (4)$$

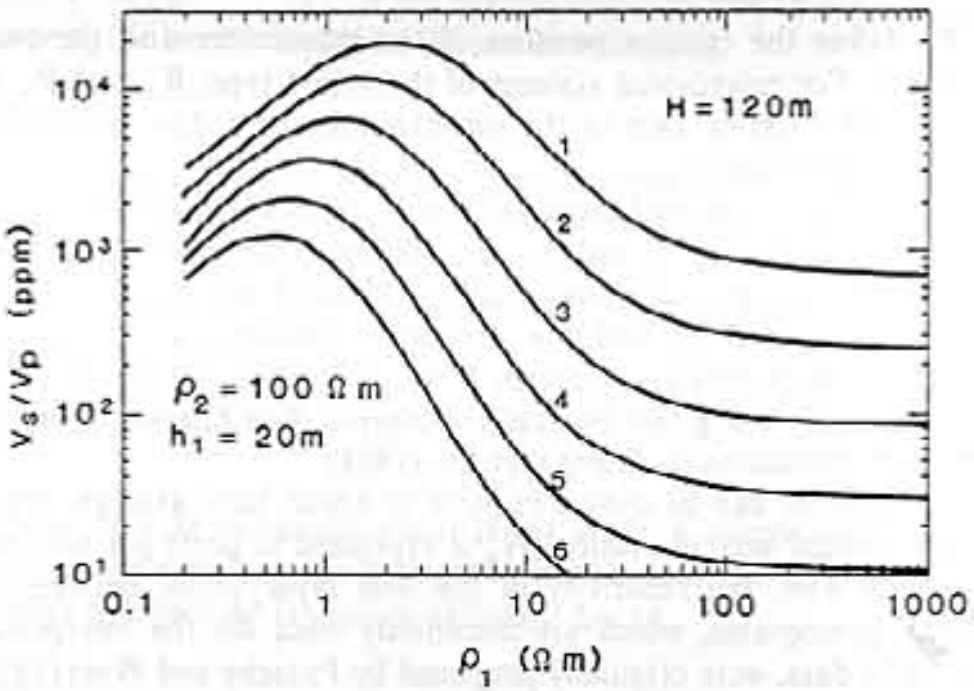

FIG. 2. Theoretical response of the AEM system sketched in Fig. 1 over a two-layer model. While the resistivity of the first layer varies, its thickness and basement resistivity are fixed. Channels 1–6 are indicated.

where S_k is the spectrum of the primary field given by

$$S_k = \frac{4\tau}{\pi T} \frac{\cos(k\omega_0 \tau/2)}{1-(k\omega_0 \tau/\pi)^2}.$$

As shown by Gupta Sarma, Maru and Varadarajan (1976) and Huang (1986), S_k is the sum of contributions due to negative and positive transmitter pulses S_k^+ and $S_k^- = S_k^+(1-\cos k\pi)$. From the nature of the cosine function it is obvious that $S_k = 2S_k^+$ for odd k and zero for even k ($k = 0, 2, 4, \ldots$). In (4), τ is the pulse width, T is the period and ω_0 is 2π times the fundamental (repetition) frequency (139 Hz for the M-1 system).

In recent years, it has become standard practice in AEM methods to express results of field surveys as V_s/V_p, the ratio of induced voltages due to secondary and primary magnetic fields at the receiver (Palacky and West 1991). In time-domain pulse AEM surveys, V_s and V_p cannot be measured simultaneously. Modern digital systems such as GEOTEM and QUESTEM monitor V_p continuously, but in surveys with the INPUT and M-1 systems, V_p was determined only sporadically and was considered constant during a survey. In the early, uncalibrated versions of the INPUT system, the output was not normalized and the secondary field was given in arbitrary units (Palacky and West 1973).

The ratio V_s/V_p has always been used in theoretical and modelling studies (Palacky 1975). The usual definition for the INPUT-type time-domain system is

$$\frac{V_s}{V_p} = \frac{2\tau\omega_0}{3\pi} \frac{(R_H^2 + R_V^2)^{3/2}}{R_H R_V} \sum_{k=1,3,\ldots}^{\infty} kS_k |D_k| \sin(k\omega_0 t + \phi_k), \qquad (5)$$

where R_H, R_V define the relative position of the transmitter and the receiver as depicted in Fig. 1. For towed-bird systems of the INPUT type, R_H and R_V are typically between 50 and 100 m. Due to the aerodynamics of a slow survey flight, the term $R_H R_V$ can never be zero.

The summation in (5) was performed for $k = 1, \ldots, 301$ (151 terms) and for delay times of $t = 0.3$, 0.5, 0.8, 1.2, 1.7 and 2.3 ms (channel settings of the M-1 system). Relative channel amplitudes were obtained for a number of first-layer resistivities, while the basement resistivity and the first-layer thickness were kept constant (100 Ωm and 20 m, respectively). The term D was defined as the integral in (1) and was solved numerically using fast Hankel transforms. The filtering coefficients for the transform were calculated by Wang and Liu (1984).

The system response can be shown in plots in which both axes are logarithmic (Fig. 2). On the vertical axis, the ratio V_s/V_p is expressed in parts per million (ppm). On the horizontal axis, the resistivity of the first layer varies between 0.1 and 1000 Ωm. Such nomograms, which are commonly used for the interpretation of time-domain AEM data, were originally proposed by Palacky and West (1973).

Damped Least-Squares Inversion with Singular Value Decomposition

In our study, a damped least-squares inversion with SVD is used. A brief outline will be given here; more details can found in Lawson and Hanson (1974) and Menke (1984). The notation used has been adopted from Pedersen and Hermance (1986) and Eysteinsson (1988).

In the first step, the data vector y is defined as a set of measured data points $(y_1, \ldots, y_N)$. The model parameter vector x is a set of unknown model parameters $(x_1, \ldots, x_M)$, thus

$$\mathbf{y} = [y_1, y_2, \ldots, y_N]^T, \tag{6}$$

$$\mathbf{x} = [x_1, x_2, \ldots, x_M]^T. \tag{7}$$

In (6) and (7), T is the transpose, N is the number of measured data points, and M is the number of model parameters. For time-domain AEM measurements using the M-1 or INPUT systems, the set of measured data are the amplitudes at six channels. For the two-layer case described here, the set of model parameters are the thickness and resistivity of the upper layer and the resistivity of the underlying medium.

The functional relationship between the model parameters and the AEM response defined in (5) can be rewritten as

$$y_i = F_i(\mathbf{x}), \qquad i = 1, \ldots, N. \tag{8}$$

For the AEM problem, the function $F_i(\mathbf{x})$ is highly non-linear. To linearize the problem locally, we expand $F_i(\mathbf{x})$ in a Taylor series around the initial model parameter vector $\mathbf{x}^0 = [x_1^0, \ldots, x_M^0]^T$ and neglect higher-order terms. Thus (8) becomes

$$(y_i - y_i^0) = \sum_{j=1}^{M} \frac{\partial F_i(\mathbf{x}^0)}{\partial x_j} (x_j - x_j^0), \tag{9}$$

where the vector $\mathbf{y}^0 = [y_1^0, \ldots, y_N^0]^T$ is the system response due to the initial model parameter vector $\mathbf{x}_0$. In matrix notation, (9) can be written as

$$\Delta \mathbf{y} = \mathbf{A}\, \Delta \mathbf{x}, \tag{10}$$

where $\Delta \mathbf{y}$ is a vector of differences between the measured data and the response of the initial model, and $\Delta \mathbf{x}$ is an unknown vector to be solved, consisting of differences between the true and initial model parameters, $\mathbf{x}$ and $\mathbf{x}^0$ respectively. The matrix $\mathbf{A}$ is referred to as the Jacobian partial derivative or sensitivity matrix. Its elements are given by

$$a_{ij} = \frac{\partial F_i}{\partial x_j}. \tag{11}$$

In general, $\mathbf{A}$ is an $N \times M$ rectangular matrix ($M \neq N$). A simple inverse operator $\Delta \mathbf{x} = \mathbf{A}^{-1}\, \Delta \mathbf{y}$ does not exist because a singular matrix does not have an inverse. A generalized inverse operator $\mathbf{A}^*$ is used to calculate $\Delta \mathbf{x}$, i.e.

$$\Delta \mathbf{x} = \mathbf{A}^*\, \Delta \mathbf{y}. \tag{12}$$

Using SVD, (12) can be written as

$$\Delta \mathbf{x} = \mathbf{V}\mathbf{S}^{-1}\mathbf{U}^T\, \Delta \mathbf{y}, \tag{13}$$

where $\mathbf{U}$ is an $N \times N$ data eigenvector matrix and $\mathbf{V}$ is an $M \times M$ model parameter eigenvector matrix. $\mathbf{U}$ and $\mathbf{V}$ are orthogonal matrices. $\mathbf{S}$ is an $N \times M$ diagonal matrix whose elements s_j are non-negative and referred to as singular values. $\mathbf{S}^{-1}$ is obtained by taking the transpose of $\mathbf{S}$ and replacing the diagonal elements with their reciprocals. If some of the singular values are zero, (13) becomes

$$\Delta \mathbf{x} = \mathbf{V}_p \mathbf{S}_p^{-1} \mathbf{U}_p^T\, \Delta \mathbf{y}, \tag{14}$$

where $\mathbf{V}_p$ and $\mathbf{U}_p$ consist of the first p columns of $\mathbf{U}$ and $\mathbf{V}$, and $\mathbf{S}_p$ of the first p rows of $\mathbf{S}$. p is the number of non-zero singular values.

The approach discussed here uses SVD with damped least-squares inversion. Therefore,

$$\Delta \mathbf{x} = \mathbf{V}_p \mathbf{S}_p (\mathbf{S}_p^2 + \varepsilon^2 \mathbf{I})^{-1} \mathbf{U}_p^T\, \Delta \mathbf{y}, \tag{15}$$

where $\mathbf{I}$ is the identify matrix and ε^2 is the damping parameter. The stochastic parameter ε is defined as a percentage of the largest singular value S_1 at each iteration. (Obviously, it changes each time.)

Using (15) and assuming $\varepsilon = 0$, the error Q, given by

$$Q = \frac{1}{N} \sum_{i=1}^{N} [y_i - F_i(\mathbf{x})]^2, \tag{16}$$

will be minimized in the least-squares sense. In the case of non-linear problems, several iterations are required before an acceptable solution is obtained in terms of minimizing the error between the measured data and the model response.

Calculation of the Jacobian matrix

The partial derivatives in (11) are calculated analytically from (1), where derivatives with respect to resistivities and thicknesses of the media involve only the term $M(\lambda)$. Thus, we can write

$$\frac{\partial M(\lambda)}{\partial x_j} = -\frac{2\lambda}{(1+\lambda C_1)^2}\frac{\partial C_1}{\partial x_j}, \qquad j = 1, 2, 3, \tag{17}$$

where x_1 and x_2 are the respective resistivities of the first layer and the basement, and x_3 is the thickness of the first layer. The derivatives of C_1 with respect to each model parameter can be obtained and substituted into (17). Partial derivatives of the AEM response with respect to model parameters can be obtained by replacing $M(\lambda)$ by (17) in (1). Since AEM data and model parameters vary over several orders of magnitude, data and model parameters have been rescaled to $\log y_i$ and $\log x_j$ using a procedure developed by Vozoff and Jupp (1974).

Partial derivatives of the AEM response with respect to the first-layer resitivity are shown in Fig. 3. The model parameters and the flight height are the same as in Fig. 2. For individual channels, a small variation in resistivity causes a large change in the measured data near minima on partial derivative curves (e.g. 10 Ωm on channel 1). Highly resistive layers are poorly resolved and resistivity determinations become impossible for values greater than 500 Ωm.

Partial derivatives of the AEM response with respect to the first-layer thickness are shown in Fig. 4. In principle, thicknesses from 10 to 50 m should be well determined on all channels. The largest partial derivative was obtained for channel 6 and thickness values of about 50 m. The observation that for higher channels maxima

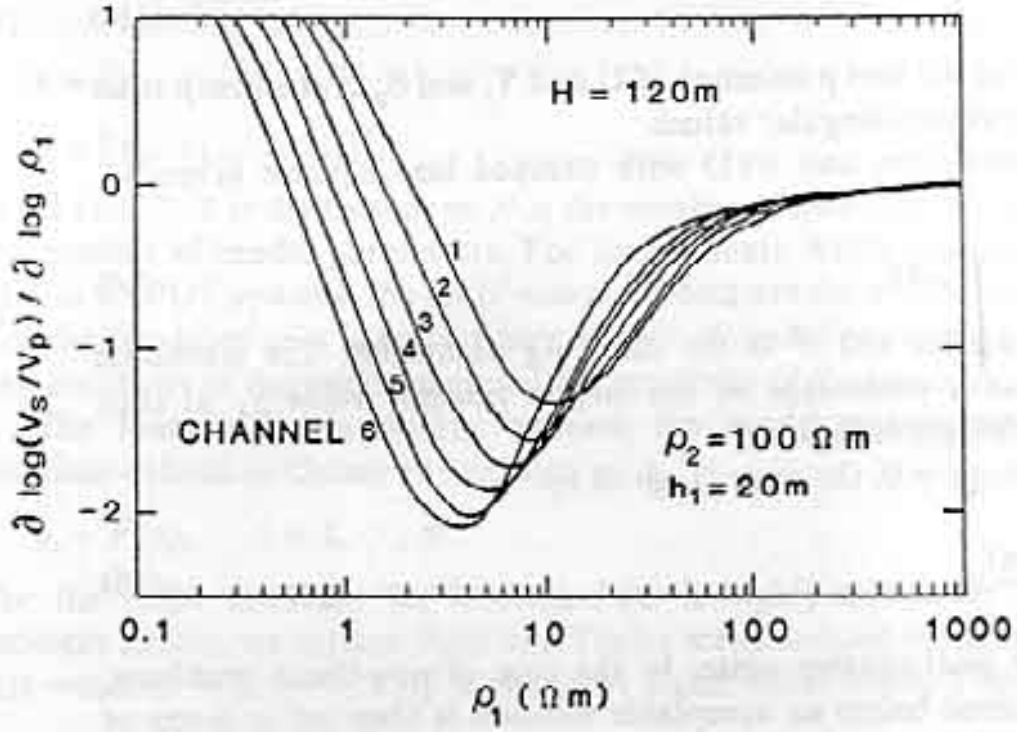

FIG. 3. Partial derivatives of the logarithm of the theoretical response (Fig. 2) with respect to the logarithm of the first-layer resistivity. Basement resistivity and the first-layer thickness were fixed.

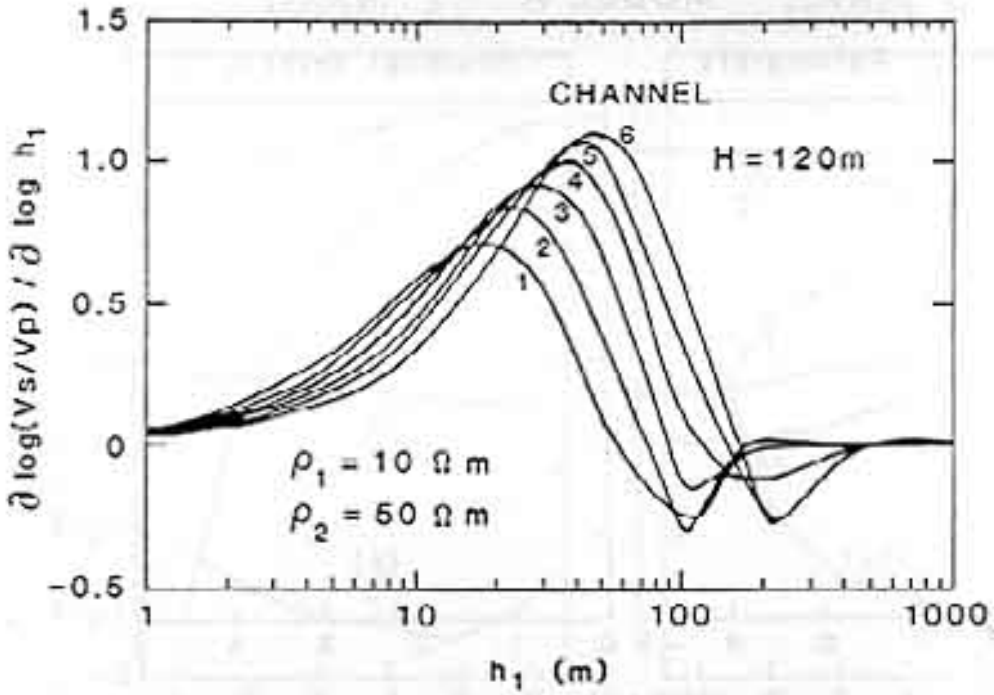

FIG. 4. Partial derivatives of the logarithm of the theoretical response with respect to the logarithm of the first-layer thickness. Resistivities of the basement and of the first layer were fixed.

are reached for greater thickness values is consistent with the well-known fact that penetration of time-domain systems increases with the delay time.

Inversion of synthetic data

The described inversion technique will be demonstrated first on synthetic, noise-free data. Several two-layer models with various combinations of resistivities (ρ_1 and ρ_2) and thickness of the first layer (h_1) have been considered.

Results obtained for two models will be discussed. Model A, in which $h_1 = 20$ m, $\rho_1 = 10\ \Omega$m and $\rho_2 = 500\ \Omega$m, simulates the common situation of conductive overburden overlying a resistive basement. In sedimentary areas, layering as in model B can be found; a moderately resistive layer overlying a conductive basement ($h_1 = 100$ m, $\rho_1 = 50\ \Omega$m, $\rho_2 = 1\ \Omega$m).

Inversion results for the two models are shown in Fig. 5. The initial inversion model was a homogeneous half-space with a resistivity of 80 Ωm (model A) and 20 Ωm (model B). Panels (a) illustrate how the three model parameters change after each iteration. Initially (iteration 1), h_1 remains the same because there is no resistivity contrast. The layer thickness approaches the true model value with a gradual change in the first-layer resistivity. For both models, acceptable values have been reached after five iterations. Panels (b) illustrate the decrease in the error Q (as defined in (16)), which is more than four orders of magnitude in four iterations. In practice, the program does not start with a homogeneous model, but with parameters determined for the previous data point, thereby reducing the time required for the inversion of a complete flight line. A similar sequential procedure was proposed by De Moully and Becker (1984) for the table look-up approach.

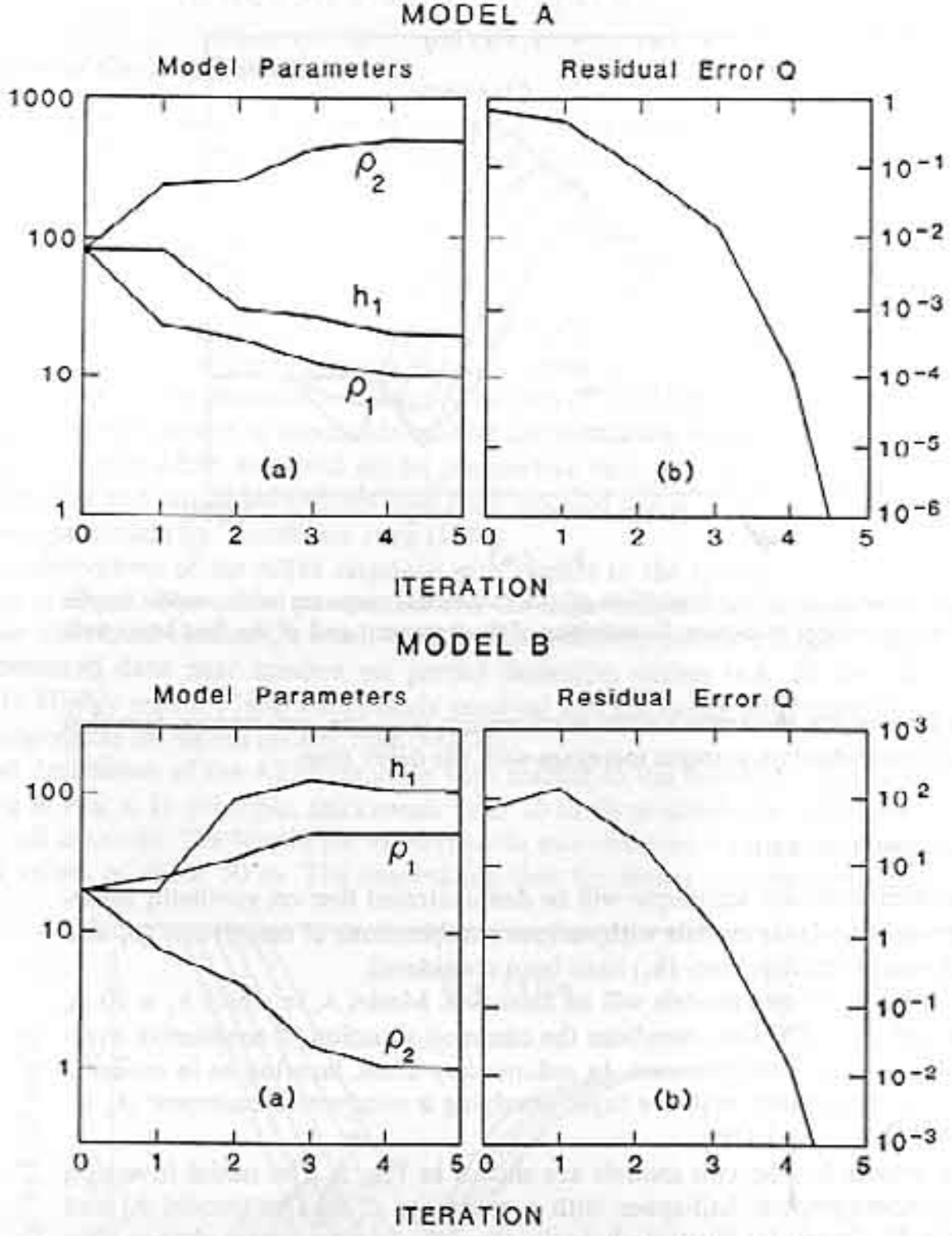

FIG. 5. Results of a least-squares inversion based on SVD for two models. The change of model parameters (a) and the associated error (b) are shown as a function of the number of iterations.

Relative importance of model parameters

The relative importance of model parameters will be evaluated for models A and B which represent extreme, but geologically plausible, situations. Figure 6 shows partial derivatives of AEM responses with respect to model parameters. For model

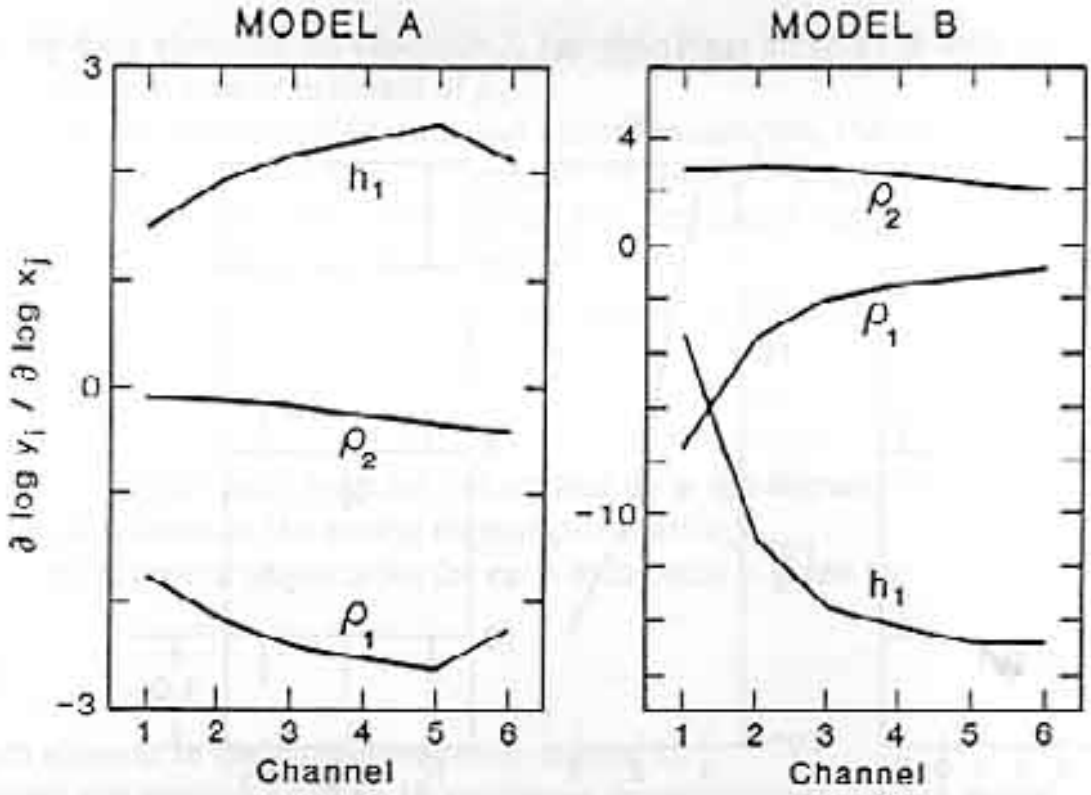

FIG. 6. Partial derivatives of the theoretical response with respect to model parameters for models A and B. Values close to zero indicate poor reliability in parameter determination.

A, the parameters h_1 and ρ_1 have a large contribution (positive or negative) and therefore can be determined accurately from the responses on all channels. However, the estimate of ρ_2 remains ambiguous in most cases (the partial derivatives are close to zero). In the case of model B, h_1 will be well determined from responses on channels 2–6; the resistivity ρ_1 affects more measurements on channel 1 than any other channel.

Figure 7 depicts three panels related to the matrices U, S and V which were defined in (13): U is the data eigenvector matrix, S is the singular value matrix and V is the model parameter eigenvector matrix. The left panels show the relative contributions of the six channels (data eigenvectors) to the three model eigenvectors, x_1, x_2, x_3. In the case of both models, all channels contribute about equally to the first data eigenvector. The model parameters mostly associated with the first data eigenvector are h_1 and ρ_1 for model A and h_1 for model B (right panel). The middle panel shows an alternative form of presenting the information in Fig. 6. For model B, h_1 is the best-determined parameter because it is asssociated with the largest singular value S_1. ρ_2 is poorly determined because it has a small singular value.

The panels in Fig. 7 show the relative contribution of individual channels to the determination of model parameters. For instance, for model B, the parameter eigenvector associated with the second singular value consists largely of ρ_1 (right panel) and its main component is the response on channel 1 (left panel). In other words, most information related to the first-layer resistivity for situations such as model B is contained in data measured on channel 1. A similar conclusion has probably been reached experimentally by many geophysicists after interpretation of field time-domain AEM data.

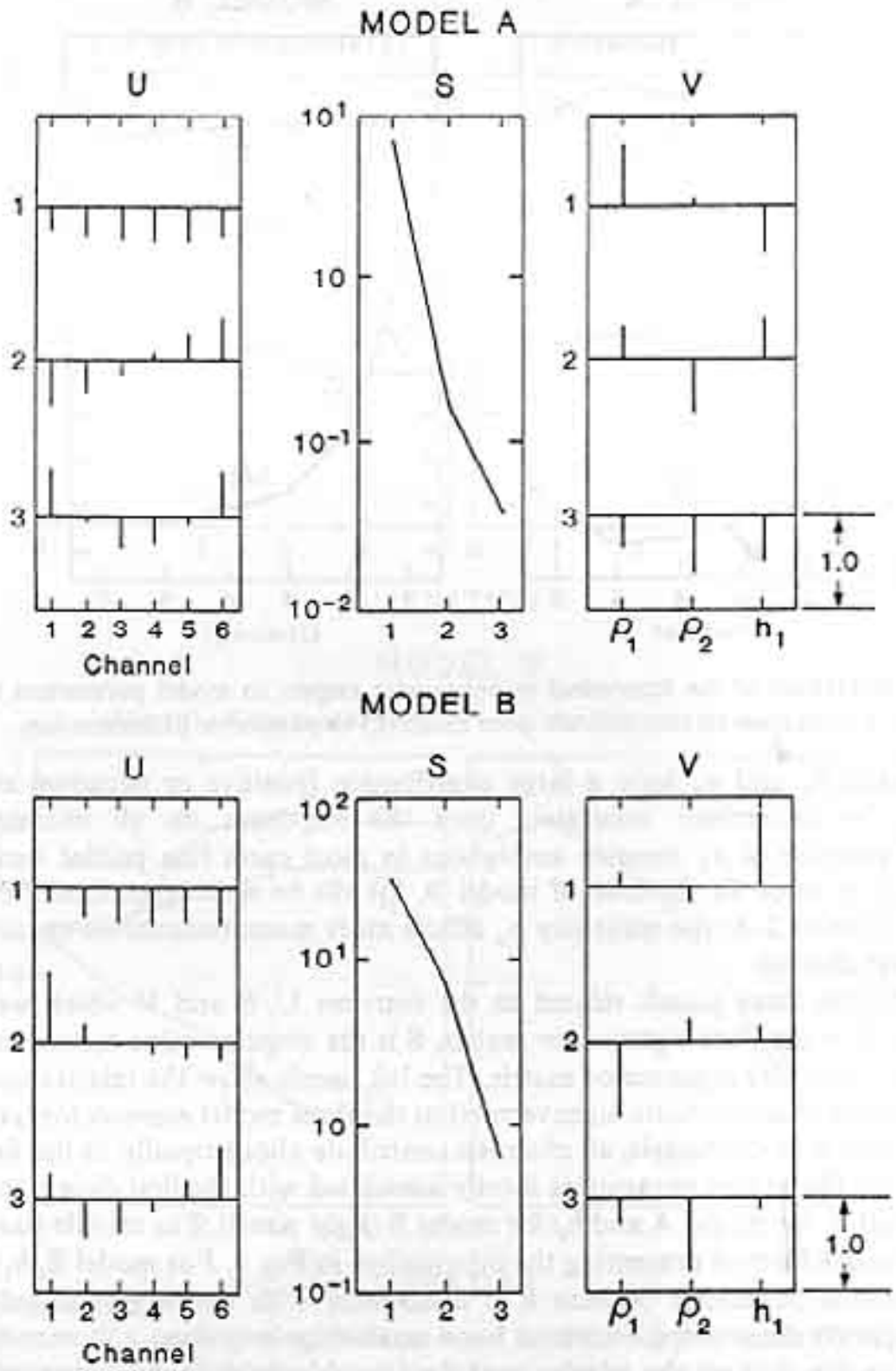

FIG. 7. Matrices of data eigenvectors (U), singular values (S), and model parameter eigenvectors (V) for models A and B.

Analysis of eigenvectors and singular values is useful for studying error propagation in the system. If channel data along which the eigenvector is principally directed are in error and if the associated singular value is small, the error is greatly magnified in the direction of the associated parameter eigenvector. For instance, for model B, the data eigenvector associated with the smallest singular value s_3 in Fig. 7

is affected mostly by data recorded on channels 2, 3 and 6. Thus an error in data on those channels will result in a poor estimate of ρ_2.

To display the relative importance of data and model parameters, the concept of 'total degree of importance' defined by Eysteinsson (1988) can be employed. While such parameters do not contain any information not previously discussed, they represent another way of assessing the relative contributions.

The total degree of importance for each model parameter is defined as

$$x_i = \sum_{j=1}^{p} v_{ij}^2 s_j, \tag{18}$$

where p is the number of non-zero singular values and v_{ij} is the element located in the ith row and the jth column in the model eigenvector matrix **V**.

Similarly, the total degree of importance for each data point is given by

$$y_i = \sum_{j=1}^{p} u_{ij}^2 s_j, \tag{19}$$

where u_{ij} is the ijth element in the data eigenvector matrix **U**.

These parameters are relative and can be expressed in percentages, e.g. for model parameters

$$x_i^p = \left(x_i \Big/ \sum_{j=1}^{M} x_j \right) 100\%.$$

The results for models A and B are listed in Table 1. For model A, the highest percentage has been obtained for ρ_1 (52.9%), closely followed by h_1 (44.2%). However, in certain situations (thin and highly conductive overburden), they cannot be resolved separately and their ratio (conductance) becomes the best-determined parameter. For model B, h_1 is the most important model parameter (75.6%). The total degree of importance of data measured at any of the six channels does not differ significantly; for model A it ranges from 21.6% on channel 5 to 9.9% on channel 1, and for model B, from 18.4% on channel 1 to 12.7% on channel 2. If all

TABLE 1. Total degree of importance.

Data	Model A	Model B
Channel		
1	9.9%	18.4%
2	14.1%	12.7%
3	17.7%	15.8%
4	19.4%	17.9%
5	21.6%	18.2%
6	17.3%	17.0%
Parameter		
ρ_1	52.9%	18.5%
ρ_2	2.9%	5.9%
h_1	44.2%	75.6%

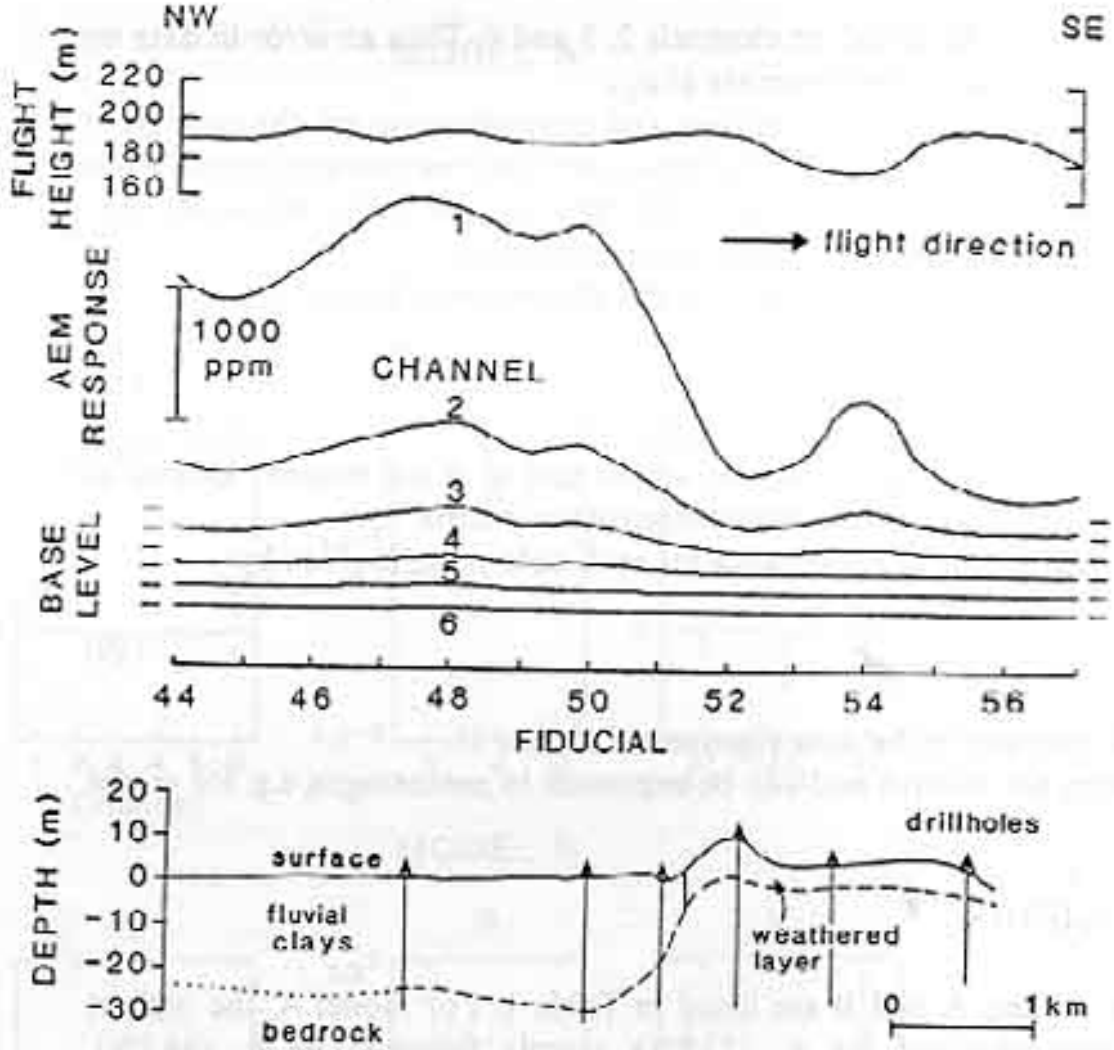

FIG. 8. AEM data and geological section from Dongling, Anhui Province, China. From the top: altimeter trace, AEM response (amplitudes measured at six channels using the M-1 system with their respective base levels), and the fiducials. In the geological section, drillhole locations and interpreted depth to bedrock (overburden thickness) are indicated.

channels are weighted uniformly in the Jacobian matrix, then they have roughly similar degrees of importance. This finding means that in a routine INPUT or M-1 survey, all channels are approximately equally important. (In this analysis, noise levels on various channels have not been taken into consideration.)

Inversion of noisy data

Field data will always contain a noise component. For the M-1 system, the noise level ranges from 100 ppm (peak to peak) on channel 1 to 5 ppm on channel 6. When values of this order of magnitude were added to the synthetic data, the number of iterations increased to six and the error Q also increased but did not exceed 15% for the well-determined parameters (ρ_1, h_1). In practice, the accuracy of determining those model parameters which are most dependent on long delay-time data, may suffer because of the sharp decline in late channel amplitudes, which are more affected by system noise.

FIELD EXAMPLE

In 1983 an AEM survey with the M-1 system was carried out near Dongling, Anhui Province. Lead–zinc mineralization of the replacement type type in Mesozoic limestones is known in the area. The purpose of the survey was to detect unknown mineralized bodies and to determine the thickness of fluvial clays in the Yangtze River plain and the extent of weathering in areas underlain by Mesozoic rocks. The flight line direction was NW–SE and the line spacing was 500 m.

Figure 8 shows M-1 data and a geological section. The M-1 data consist of (from the top): the altimeter trace; measured amplitudes at six channels with indicated base levels; fiducials (one unit equals approximately 500 m). The geological section was obtained by interpolation of drilling data. The locations of drill holes are indicated in the figure. The section shows a contact between thick Cenozoic clays of fluvial origin and a much thinner weathered layer formed over Mesozoic rocks (mostly limestones with minor shale). Ground resistivity surveys were used to determine resistivities and thicknesses of individual layers. The resistivity of fluvial clays was interpreted to be between 5 and 15 Ωm, that of the weathered layer somewhat higher, up to 50 Ωm. The underlying Mesozoic strata were found to have resistivities of hundreds to thousands of Ωm. Strong AEM anomalies are due to conductive fluvial clays. A peak near fiducial 54 probably reflects a change in the flight height.

Figure 9 shows the inversion results for the same line segment. The apparent

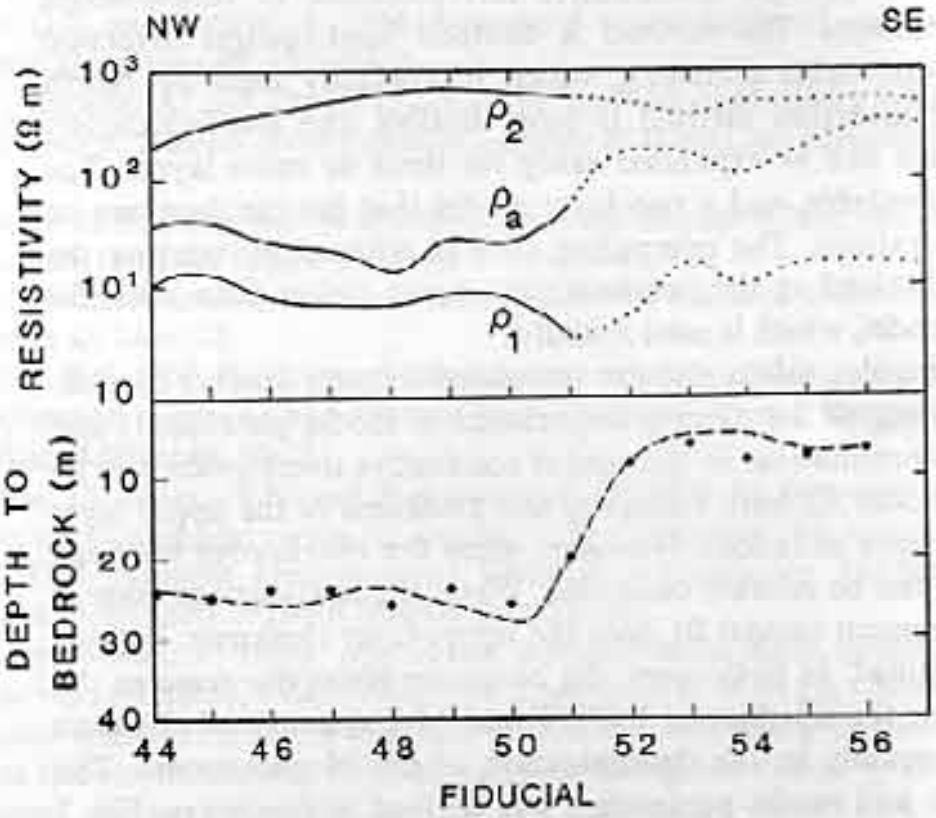

FIG. 9. Top: Traces of apparent resistivity (ρ_a) and first- and second-layer resistivities (ρ_1 and ρ_2) obtained by inversion of the AEM data shown in Fig. 8. Bottom: depth to bedrock interpreted from drilling (dashed line) and inversion of AEM data at each fiducial (dots).

resistivity (ρ_a) curve was obtained by inversion of AEM data at six channels, assuming a homogeneous half-space model. This parameter is frequently depicted in maps resulting from AEM surveys. A sharp increase in the apparent resistivity near fiducial 51 marks the transition from fluvial clays to Mesozoic sediments. A dotted curve over the southeast portion of the profile indicates less reliable results due to the relatively high noise level of the system, whose effect on inversion is greater when the amplitudes are small, particularly on later channels.

Inversion assuming a two-layer model yielded information which was geologically more meaningful. As expected, there was not much variation in the resistivity of the underlying Mesozoic strata (200–700 Ωm). The resistivity of the first layer was found to be somewhat lower over Cenozoic fluvial clays (5–12 Ωm) than over weathered Mesozoic sediments (about 20 Ωm). These values agree well with the previously-mentioned sounding results. The most diagnostic result was the depth to bedrock. There is very good agreement between the depth interpreted from drilling data (dashed line) and the results of inversion (solid circles). A high degree of accuracy in determining overburden thickness was predicted by the previously-described analysis of the relative importance of model parameters.

Conclusions

A technique has been developed for quantitative interpretation of time-domain towed-bird AEM measurements. The method is damped least-squares inversion with SVD. Unlike computer table matching, which is normally used by North American contractors, an inversion method is more flexible and mathematically more elegant. The approach can be expanded easily for three or more layers. The algorithm described is dependable, and a two-layer model that fits the data can be obtained in only a few iterations. The computing time is reduced by starting the inversion with a model obtained at the previous data point rather than with the homogeneous half-space model, which is used initially.

The analysis made of singular values and the associated singular vectors contributes to a better understanding of the relative importance of model parameters and of the reliability of their determination. In the case of conductive overburden overlying a resistive basement (model A), both resistivity and thickness of the upper layer can be well determined in most situations. However, when the overburden becomes thin, only its conductance can be reliably estimated. When the near-surface layer is more resistive than the basement (model B), only the upper-layer thickness, but not its resistivity, is well determined. In both cases, the basement resistivity remains the least reliable parameter. For the six-channel INPUT and M-1 systems, all channels contribute approximately equally to the determination of model parameters. The relative importance of data and model parameters was derived in two ways (Fig. 7 and Table 1).

The proposed inversion method was tested on M-1 field data from Anhui Province, China. The obtained depth-to-bedrock profile compares favourably with the results of drilling and the resistivity information largely agrees with the results of ground resistivity soundings.

ACKNOWLEDGEMENTS

H.H. acknowledges the assistance of Professor J. F. Hermance, who provided computing funds, and Messrs Warren Slocum, Weizhong Wang and Greg Neumann, with whom he had useful discussions during a fellowship tenure at Brown University, Providence, Rhode Island, U.S.A. G.J.P. thanks Changchun University of Earth Sciences for hospitality during his stay in China. The authors are grateful to Dr J. O. Barongo of the University of Nairobi, Dr P. B. Keating and Dr A. K. Sinha, both of the Geological Survey of Canada, for critically reading the manuscript. Thanks are also due to two anonymous reviewers for their useful suggestions.

Geological Survey of Canada Contribution No. 41589.

REFERENCES

BARONGO, J.O. 1989. Application of transient airborne electromagnetic and ground resistivity methods to geological mapping in tropical terrains. Ph.D. thesis, McGill University, Montreal.

BAUDOIN, P., DUROZOY, G. and UTARD, M. 1970. Étude par prospection électromagnétique aérienne d'un contact eau douce – eau salée dans le delta du Rhône. In: *Mining and Groundwater Geophysics*. L. W. Morley (ed.), Geological Survey of Canada, Economic Geology Report **26**, 626–637.

BECKER, A. 1969. Simulation of time-domain, airborne, electromagnetic system response. *Geophysics* **34**, 739–752.

COLLETT, L.S. 1986. Development of the airbone electromagnetic technique. In: *Airborne Resistivity Mapping*. G. J. Palacky (ed.), Geological Survey of Canada Paper **86-22**, 9–18.

DE MOULLY, G.T. and BECKER, A. 1984. Automated interpretation of airborne electromagnetic data. *Geophysics* **49**, 1301–1312.

DYCK, A.V., BECKER, A. and COLLETT, L.S. 1974. Surficial conductivity mapping with the INPUT system. *Bulletin of the Canadian Institute of Mining and Metallurgy* **67-774**, 104–109.

EYSTEINSSON, H. 1988. The inversion of two-dimensional magnetotelluric and magnetic variation data. Ph.D. thesis, Brown University, Providence, R.I.

FRASER, D.C. 1978. Resistivity mapping with an airborne multicoil electromagnetic system. *Geophysics* **43**, 144–172.

FRISCHKNECHT, F.C. 1967. Fields about an oscillating magnetic dipole over a two-layer earth and application to ground and airborne electromagnetic surveys. *Quarterly of the Colorado School of Mines* **62**, No. 1.

GUPTA SARMA, D., MARU, V.N. and VARADARAJAN, G. 1976. An improved pulse transient airborne electromagnetic system for locating good conductors. *Geophysics* **41**, 287–299.

HUANG, H. 1986. *Airborne Electromagnetic Methods in Geophysics*. Publishing House of Changchun University of Earth Sciences [in Chinese].

HUANG, H. and WANG, Y. 1985a. Application of time-domain AEM systems to reconnaissance survey of coalfield. *Coal Geology and Exploration* **5**, 49–54 [in Chinese].

HUANG, H. and WANG, Y. 1985b. A computer method of transforming the time-domain AEM response into apparent resistivity. *Journal of the Changchun College of Geology* **4**, 85–92 [in Chinese, abstract in English].

HUANG, H., XI, H., WANG, Y., ZHU, D. and PIAO, H. 1983. Transformation of time-domain AEM response to apparent resistivity and its application in geological mapping. *Journal of the Changchun College of Geology* **3**, 135–144 [in Chinese, abstract in English].

JACKSON, D.J. 1972. Interpretation of inaccurate, insufficient and inconsistent data. *Geophysical Journal of the Royal Astronomical Society* **27**, 97–109.

KEATING, P.B. and CROSSLEY, D.J. 1990. The inversion of time-domain airborne electromagnetic data using the plate model. *Geophysics* **55**, 705–711.

KOVACS, A., VALLEAU, N. and HOLLADAY, J.S. 1987. Airborne electromagnetic sounding of ice thickness and sub-ice bathymetry. *CREEL Report* **87-23**, 1–40. US Army Corps of Engineers, Cold Regions Research and Engineering Laboratory.

LAWSON, C.L. and HANSON, R.J. 1974. *Solving Least-Squares Problems*. Prentice Hall, Inc.

MACNAE, J.C. 1979. Kimberlites and exploration geophysics. *Geophysics* **34**, 1395–1416.

MENKE, W. 1984. *Geophysical Data Analysis: Discrete Inverse Theory*. Academic Press, Inc.

NELSON, P.H. and MORRIS, D.B. 1969. Theoretical response of a time-domain, airborne, electromagnetic system. *Geophysics* **34**, 729–738.

O'CONNELL, M.D. and NADER, G.L. 1986. Conductive layer mapping by computer processing of airborne electromagnetic measurements. In: *Airborne Resistivity Mapping*. G. J. Palacky (ed.), Geological Survey of Canada Paper **86-22**, 111–124.

PALACKY, G.J. 1975. Interpretation of Input AEM measurements in areas of conductive overburden. *Geophysics* **40**, 490–502.

PALACKY, G.J. 1981. The airborne electromagnetic method as a tool of geological mapping. *Geophysical Prospecting* **29**, 60–88.

PALACKY, G.J. 1986. Airborne electromagnetics at crossroads. In: *Airborne Resistivity Mapping*. G. J. Palacky (ed.), Geological Survey of Canada Paper **86-22**, 5–8.

PALACKY, G.J. 1987. Clay mapping using electromagnetic methods. *First Break* **5**, 295–306.

PALACKY, G.J. and WEST, G.F. 1973. Quantitative interpretation of Input AEM measurements. *Geophysics* **38**, 1145–1158.

PALACKY, G.J. and WEST, G.F. 1991. Airborne electromagnetic methods. In: *Electromagnetic Methods in Applied Geophysics*. M. N. Nabighian (ed.), **2**, *Investigations in Geophysics* **6**, Society of Exploration Geophysicists (in press).

PATERSON, N.R. and REFORD, S.W. 1986. Inversion of airborne electromagnetic data for overburden mapping and groundwater exploration. In: *Airborne Resistivity Mapping*. G. J. Palacky (ed.), Geological Survey of Canada Paper **86-22**, 39–48.

PEDERSEN, J. and HERMANCE, J.F. 1986. Least-squares inversion of one-dimensional magnetotelluric data: an assessment of procedures employed by Brown University. *Surveys in Geophysics* **8**, 187–231.

VOZOFF, K. and JUPP, L.B. 1974. Joint inversion of geophysical data. *Geophysical Journal of the Royal Astronomical Society* **42**, 977–991.

WAIT, J.R. 1958. Induction by an oscillating magnetic dipole over a two-layer ground. *Journal of Applied Science Research* **B-7**, 73–80.

WANG, Y. and LIU, H. 1984. Analytical calculation of filtering coefficients for fast Hankel transforms. *Proceedings of Symposium on Electrical Soundings, Beijing* [in Chinese].

WARD, S.H. 1971. Electromagnetic theory for geophysical applications. In: *Mining Geophysics*. S. H. Ward (ed.), **2**, 13–196. Society of Exploration Geophysicists.

WARD, S.H. and HOHMANN, G.W. 1988. Electromagnetic theory for geophysical applications. In: *Electromagnetic Methods in Applied Geophysics*. M. N. Nabighian (ed.), **1**, 130–311, *Investigations in Geophysics* **3**, Society of Exploration Geophysicists.

WIGGINS, R.A. 1972. The general linear inverse problem: Implications of surface waves and free oscillations for earth structure. *Reviews of Geophysics and Space Physics* **10**, 251–285.

ZHENG, X. and WANG, Y. 1979. Airborne electromagnetic system (pulse type) and its application in geological mapping and prospecting. *Journal of the Changchun Geological Institute* **3**, 98–105 [in Chinese].

ZOLLINGER, R., MORRISON, H.F., LAZENBY, P.G. and BECKER, A. 1987. Airborne electromagnetic bathymetry. *Geophysics* **52**, 1127–1137.